A&A 493, 687–696 (2009)
DOI: 10.1051/0004-6361:200810712

Astronomy & Astrophysics

Rotational excitation of formaldehyde by hydrogen molecules: ortho-H_2CO at low temperature⋆,⋆⋆

N. Troscompt, A. Faure, L. Wiesenfeld, C. Ceccarelli, and P. Valiron

Laboratoire d'Astrophysique de Grenoble, UMR 5571-CNRS, Université Joseph Fourier, Grenoble, France
e-mail: afaure@obs.ujf-grenoble.fr

Received 30 July 2008 / Accepted 15 October 2008

ABSTRACT

Aims. Rate coefficients for the rotational excitation of the ten lowest levels of ortho-H_2CO by collisions with H_2 molecules are computed for kinetic temperatures in the range 5−100 K.
Methods. Cross sections are obtained from extensive, fully converged, quantum-mechanical scattering calculations using a highly accurate potential energy surface computed at the CCSD(T) level with a basis set extrapolation procedure. Scattering calculations are carried out for H_2 molecules in both para and ortho rotational levels.
Results. The present rates are shown to differ significantly from those available in the literature. Moreover, the strength of propensity rules is found to depend on the para/ortho form of H_2. Radiative transfer modeling also shows that the new rates have a significant impact on H_2CO emission line fluxes and that they should be adopted in any detailed radiative transfer model of ortho-H_2CO in cold environments ($T \lesssim 30$ K).

Key words. molecular data – molecular processes – ISM: molecules

1. Introduction

Formaldehyde (H_2CO) was the first organic polyatomic molecule discovered in the interstellar medium at the end of the sixties (Snyder et al. 1969). Since then it has been extensively observed both in galactic and extragalactic sources. Many reasons make the observation of formaldehyde in space important, but all can be summarized in one sentence: *observation of formaldehyde rotational lines is one of the best tools we have for studying astrophysical sources*. First, the relatively large dipole moment and abundance of the molecule make the rotational lines relatively easy to observe from ground-based observations. Indeed, formaldehyde lines have been detected in a variety of astronomical sources: from comets in the Solar System (e.g. Fray et al. 2006) to the coldest objects of our Galaxy, the pre-stellar cores (Bacmann et al. 2003), and up to distant starburst galaxies (Mangum et al. 2008). Formaldehyde rotational lines are observed in diffuse (Liszt et al. 2006) and in dense (Minh et al. 1993) molecular clouds, in massive (van der Tak et al. 2000) and in low-mass protostars (Maret et al. 2004). In short, rotational lines from formaldehyde are observed everywhere in space. Yet, what makes formaldehyde rotational lines such a popular and powerful tool for studying astronomical sources is their valuable diagnostic capabilities. The most important is the ability of formaldehyde rotational lines to constrain the density of the studied source (e.g. Mangum & Wootten 1993). This is due to the structure of H_2CO, a slightly asymmetric rotor, which leads to a "K-doublet" structure of the rotational energy levels. Very generally speaking, observations of transitions from different ΔK transitions turn out to be very powerful constraints on the gas-emitting density. This property has been widely used in the literature to derive the density of several astronomical sources. Actually, observations of carefully selected H_2CO rotational lines (namely spanning a wide enough range of upper energy level and spontaneous emission coefficient) can be used to reconstruct the density profile and the H_2CO abundance profile of the studied source (e.g. Ceccarelli et al. 2003). We mention here one specific example to illustrate this point. In low-mass protostars, multi-frequency observations of H_2CO have permitted discovery of the *hot corinos*, warm and dense regions inside the cold envelopes of Class 0 sources where the abundance of formaldehyde jumps by more than a factor of 100 (Ceccarelli et al. 2000, 2001; Maret et al. 2004). At the same time, the abundances of several complex organic molecules also show a jump (Cazaux et al. 2003). This allows us to introduce another important aspect of H_2CO observations: formaldehyde is the simplest and often most abundant polyatomic organic molecule containing oxygen observed in space. It is considered a "parent molecule" from which more complex organic molecules spring (e.g. Charnley et al. 1997). Formaldehyde is, therefore, a basic molecule of organic chemistry in space.

All the studies based on the observations and interpretation of the formaldehyde rotational lines rely on knowing of the *H_2CO collisional coefficients*, which permit observed line intensities to be "converted" into densities and abundances. These coefficients are extremely difficult to measure via laboratory

⋆ This paper is dedicated to the memory of our friend and colleague, Pierre Valiron, who died on 31 August 2008.
⋆⋆ Table of rate coefficients is available in electronic form at the CDS via anonymous ftp to cdsarc.u-strasbg.fr (130.79.128.5) or via
http://cdsweb.u-strasbg.fr/cgi-bin/qcat?J/A+A/493/687

experiments, and the best way is to compute them following the quantum scattering theory. These calculations are computationally very expensive, so for a long time, approximations have been used. However, given the huge importance that formaldehyde rotational lines have in several fields of astrophysics, it is time now to reconsider more accurate and reliable calculations. This is the goal of this article.

Hydrogen molecules are generally the most important colliding partners in the interstellar medium, although collisions with H, He, and electrons (and H_2O in comets) may be important. The very first collisional calculation on H_2CO was presented by Townes & Cheung (1969), in a purely classical framework. The first semi-classical calculations were performed by Augustin & Miller (1974) (see however Faure & Wiesenfeld 2004, for some limitations) for the system H_2CO – He. Eventually, the first fully quantum calculations were performed by Garrison et al. (1975) and Garrison et al. (1976) for 16 energy levels of ortho-H_2CO and for scattering energies between 20 and 95 K, using the H_2CO–He potential energy surface (PES) of Garrison & Lester (1975). Green et al. (1978), and more recently Green (1991), extended those calculations to 81 rotational levels and kinetic temperatures up to 300 K, still using the PES of Garrison & Lester (1975). In all these theoretical studies, He was employed as a substitute for H_2 to reduce the cost of the computations. As a result, rates for excitation by H_2 have been obtained so far by scaling the rates for He by a factor of ∼1.4, accounting for the lower reduced mass of the H_2CO–H_2 system. Recently, this approximation has been questioned experimentally at low temperatures by Mengel & De Lucia (2000). These authors have found that pressure broadening cross sections for H_2CO–H_2 are generally larger by a factor of 2 than the cross sections for H_2CO–He, suggesting a scaling factor of ∼2.8 for the rate coefficients. In the case of water, even greater differences between H_2 and He were observed, especially when H_2 is in excited rotational levels (see Faure et al. 2007, and references therein). These results suggest that the substitution of H_2 by He is very approximate and that proper H_2CO–H_2 calculations are necessary. We note finally that cross sections for electron-impact rotational excitation of H_2CO have been recently reported (Kaur & Baluja 2005).

In the present work, a high-accuracy intermolecular PES for the H_2CO–H_2 system is determined (Sect. 2.1). To the best of our knowledge, this is the first available PES for the H_2CO–H_2 system. With the help of this PES, precise quantum scattering calculations are carried out (Sect. 2.2) and collisional cross sections and rate coefficients are obtained and compared to previous H_2CO–He results (Sect. 3). In the last section we examine the influence of these new rates on the H_2CO emission line fluxes (Sect. 4).

2. Method

2.1. Potential energy surface

In the present work, we focus on the low kinetic temperature regime (5–100 K) for which the relevant collisional energies are well below the first vibrational excitation threshold of H_2CO (ν_4 = 1167 cm^{-1}, corresponding to the out-of-plane bending mode (Clouthier & Ramsey 1983)). The colliding partners may thus be safely assumed to be rigid in order to restrict the dimensionality of the intermolecular potential to five degrees of freedom (see below). An outline of the PES computation is given below, while a detailed presentation will be published in a forthcoming article.

It has been shown recently by Faure et al. (2005) for the H_2O-H_2 system that employing state-averaged geometries is a very good approximation for including vibrational effects within a rigid-rotor PES (see also Jankowski & Szalewicz 2005; Valiron et al. 2008). In the present work, the ground-state average structure of H_2CO has been taken from Duncan (1974): r_{CH} = 1.1171 Å, r_{CO} = 1.2072 Å and $\widehat{HCH}$ = 116° 14′. The ground-state average geometry of H_2 has been taken from Faure et al. (2005): r_{HH} = 1.448761 Å. We have used the conventions of Phillips et al. (1994) in defining the H_2CO–H_2 rigid-rotor coordinate system: the intermolecular potential is described as a function of five coordinates, namely the intermolecular distance R from the H_2CO center of mass to the H_2 center of mass, and four relative angles (θ, ϕ) and (θ', ϕ') which describe, respectively, the collision direction and the H_2 orientation relative to the H_2CO body-fixed system.

The five-dimensional H_2CO–H_2 surface has been constructed using the following two-step procedure: *(i)* a reference PES was computed from a large set (48 000 points) of "medium accuracy" CCSD(T) calculations using the Dunning's correlation consistent aug-cc-pVDZ basis set; *(ii)* this reference surface was subsequently calibrated using a complete basis set (CBS) extrapolation procedure based on a smaller set (8000 points) of CCSD(T)/aug-cc-pVTZ calculations. The CBS-type extrapolation was applied to the correlation part of the interaction energy and was performed using a two-point X^{-3} type extrapolation, where X is the cardinal number corresponding to the basis set, as described in Jankowski & Szalewicz (2005) (see also references therein). The self-consistent field (SCF) contribution was not extrapolated and aug-cc-pVTZ values were used. All basis sets were supplemented with midbond functions (Williams et al. 1995) and all calculations counterpoise-corrected as in Jankowski & Szalewicz (2005). The strategy of splitting the calculations into two levels of accuracy was necessary because of the large number of grid points that had to be computed and the computational cost of CCSD(T)/aug-cc-pVTZ. All correlated calculations were frozen core with negligible impact on PES accuracy.

Grid points were chosen for 22 fixed intermolecular distances R (in the range 4–15 a_0) *via* random sampling for the angular coordinates of H_2 relative to H_2CO. At each intermolecular distance, the interaction energy was then least-square fitted using a 146-term expansion for the angular coordinates, using Eq. (3) of Phillips et al. (1994). This expansion includes anisotropies up to l_1 = 13 and l_2 = 4, where the integer indices l_1 and l_2 refer to the tensor ranks of the angular dependence of the H_2CO and H_2 orientation, respectively. The CBS correction was fitted over a subset of only 49 angular terms. The accuracy of the angular expansion was monitored using a self-consistent Monte Carlo error estimator, as done previously for H_2O–H_2 (Faure et al. 2005; Valiron et al. 2008) and CO–H_2 (Wernli et al. 2006). A cubic spline interpolation was finally employed over the whole intermolecular distance range and was smoothly connected with standard extrapolations to provide continuous radial expansion coefficients suitable for scattering calculations. The accuracy of the final five-dimensional fit was found to be better than 1 cm^{-1} in the long-range and minimum region of the interaction (R > 6 bohrs), as illustrated by the rms fit error in Fig. 1.

The accuracy of the above procedure was also checked against a few number (70) of "high-cost" CCSD(T)-R12 calculations using adequate R12 suited basis sets. The particular advantage of the R12 method is to offer a direct way of reaching the basis set limit value within a single calculation, that is,

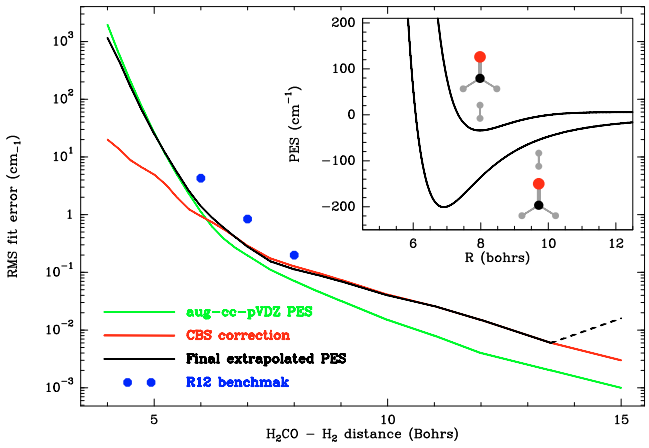

Fig. 1. Root-mean-square residual between angular fits and ab initio input data as a function of the intermolecular separation. The green line denotes the rms error for the reference (CCSD(T)/aug-cc-pVDZ) PES (146-term expansion), while the red line gives the rms for the CBS correction (49-term expansion). The rms error between the final fit and the CBS-extrapolated PES is given as the black line. The blue circles denote the rms error between the final fit and benchmak CCSD(T)-R12 values (a total of 70 R12 points were employed: 50 at 6 bohrs, 10 at 7 bohrs, and 10 at 8 bohrs). The inset shows the interaction energy as a function of the intermolecular separation for two planar H_2CO–H_2 configurations.

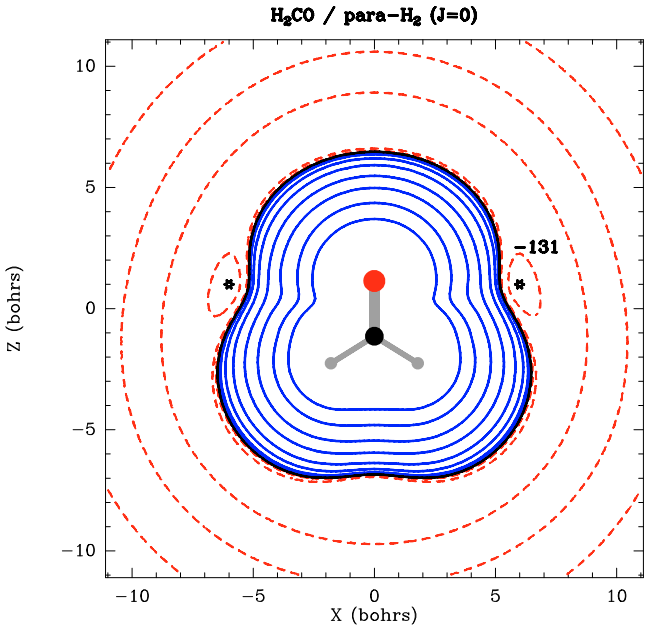

Fig. 2. Contour plots of the $H_2CO - H_2(J_2 = 0)$ PES when H_2 lies in the H_2CO plane. The H_2CO molecule is shown to scale. Equipotentials (in cm^{-1}): in dashed red, −100, −30, −10, −3; in solid black, 0; in blue 3, 10, 30, 100, 300, 1000, 3000, 10 000. The stars denote the minimum in this configuration, see text for details.

without extrapolation (Noga & Kutzelnigg 1994). As shown in Fig. 1, in the attractive part of the interaction ($R \geq 7$ bohrs), the rms error between the final fit and benchmak CCSD(T)-R12 values is lower than 1 cm^{-1}, which is the typical intrinsic accuracy of CCSD(T) calculations at the basis set limit (e.g. Noga et al. 2006). At shorter distance ($R < 6$ bohrs), the rms error increases sharply owing to steric hindrance problems, as discussed by Wernli et al. (2007a,b) for HC_3N–H_2. It can also be noticed that the rms increases above $R = 13.5$ bohrs as a result of the long-range extrapolation procedure.

A two-dimensional plot of the H_2CO–H_2 PES is presented in Fig. 2. In this plot, the interaction potential is spherically averaged over (θ', ϕ'), that is, over H_2 rotational motion. This is equivalent to constraining H_2 in its lowest para, $J_2 = 0$, rotational level (J_2 is the H_2 angular momentum). The global minimum of this averaged PES, as deduced from our fit, lies at -131 cm^{-1} for $R = 6.1$ bohrs and $(\theta, \phi) = (81°, 0°)$. In this configuration, para-H_2($J_2 = 0$) lies in the H_2CO plane and forms an approximatively T-shape arrangement with respect to the CO bond. It is interesting to compare this result with the recent high-accuracy ab initio calculations of Wheeler & Ellis (2003) on the H_2CO–He system. These authors have found the global minimum of the H_2CO–He PES at similar values of R (5.8 bohrs) and (θ, ϕ) (83°, 0°) but with a much lower intermolecular energy: −59.5 cm^{-1}. This suggests that using an He interaction to represent an orientation average of the interaction with H_2 is quite inaccurate. Note that the PES of Garrison & Lester (1975), employed in all previous scattering calculations, had a global minimum at a similar location but an even smaller intermolecular energy (∼25 cm^{-1}). Furthermore, we emphasize that the global minimum of the H_2CO–H_2 full PES, as deduced from our fit, lies at -321 cm^{-1} for $R = 5.6$ bohrs, $(\theta, \phi) = (80°, 0°)$, and $(\theta', \phi') = (118°, 0°)$. The H_2CO–H_2 system thus has a much deeper binding energy than the H_2CO–He system. Significant differences between He and H_2 inelastic rate coefficients are thus expected, especially at low temperatures where the potential well can have a spectacular effect on scattering cross sections (see e.g. Wernli et al. 2006; Dubernet et al. 2006; Faure et al. 2007; Lique et al. 2007).

2.2. Quantum scattering calculations

The slightly asymmetric top molecule H_2CO has three distinct rotational constants. In the following, rotational energy levels are labelled by three numbers: the angular momentum J and the pseudo-quantum numbers K_a, K_c, which correspond to the projection of J along the inertia a and c axis. Owing to the two H atoms of nuclear spin 1/2, H_2CO presents two spin modifications: para (total hydrogen nuclear spin 1) and ortho (total hydrogen nuclear spin 0). The para-form corresponds to K_a even and the ortho-form to K_a odd. In the following, we focus only on the ortho-H_2CO. Indeed, scattering calculations can be done separately for the different nuclear spin combinations because inelastic (nonreactive) collisions cannot interconvert the para- and ortho-forms. Kinetic temperatures are also restricted to the range 5–100 K, and finally, only the first ten levels of ortho-H_2CO are considered (see Fig. 3). It should be noted that the ground rotational state of ortho-H_2CO is 1_{11}, which lies 10.7 cm^{-1} above the ground rotational state of para-H_2CO 0_{00}. In Fig. 3 and hereafter, the ground rotational state 0_{00} is taken as the origin of the rotational energies of H_2CO in order to follow the astronomical conventions.

All cross section calculations were performed with the MOLSCAT code (Hutson & Green 1994), in the rigid rotor approximation (parameter *ITYPE = 4*). The reduced mass of the system is 1.889053 a.m.u. and the rotational constant of H_2 was taken as $B_{H_2} = 60.853$ cm^{-1}. Rotational energies and wavefunctions for H_2CO were obtained from the three rotational constants $A = 1.134191$ cm^{-1}, $B = 1.295431$ cm^{-1}, $C = 9.405525$ cm^{-1}

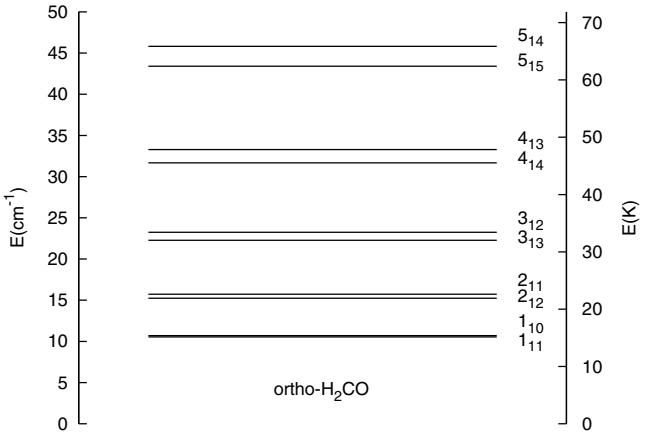

Fig. 3. Energy levels of ortho-H_2CO below 50 cm^{-1} (to scale). The ground rotational state 0_{00} of para-H_2CO is taken as the origin of the rotational energies. Quantum numbers: $J_{K_aK_c}$, see text for details.

Table 1. Details of the quantum MOLSCAT cross section calculation parameters for ranges of the total energy $E = E_{\rm rot}$ (H_2CO)+$E_{\rm rot}$ (H_2)+$E_{\rm coll}$. CC: close-coupling, CS: coupled-states approximation.

E (cm^{-1})	energy step (cm^{-1})	method
$\sigma_{jj'}(E)$ ortho-H_2CO – para-H_2 collisions		
10.7 → 55.7	0.25	CC
55.7 → 84.7	0.5	CC
84.7 → 140.7	2	CC
140.7 → 312.7	2	CS
350.7 → 1100.7	50	CS
$\sigma_{jj'}(E)$ ortho-H_2CO – ortho-H_2 collisions		
132.3 → 177.3	0.25	CC
177.3 → 207.3	0.5	CC
207.3 → 262.3	2	CC
262.3 → 432.3	2	CS
432.3 → 1132.3	50	CS

(Bocquet 1996). Close-coupling (CC), and coupled-states (CS) calculations were performed using the hybrid modified log-derivative/Airy propagator (Alexander & Manolopoulos 1987) to integrate the coupled equations. We note that the MOLSCAT parameter *STEPS* was increased up to 250 at the lowest energies to constrain the step length of the integrator below ~0.1 bohrs, in order to properly follow the details of the radial fitting coefficients. Other propagation parameters were taken as the MOLSCAT default values.

For para-H_2 calculations, the inclusion of the $J_2 = 2$ level of H_2 was necessary to obtain cross sections converged to better than 5%, even when this level was energetically closed. For ortho-H_2 calculations, however, the $J_2 = 3$ level of H_2 was found to be unnecessary for reaching a comparable convergence (at the investigated collisional energies), and only the $J_2 = 1$ level was included. For the rotational basis of H_2CO, we found it necessary to systematically include 4 J values beyond the highest open J value. As a result, the largest basis included all states up to $J = 9$, that is a total of 50 levels. Note that the largest basis (28 levels) used by Green et al. (1978) was found here to be inadequate for giving cross sections within 10% of the infinite basis limit, in particular for the smaller cross sections. The energy grid was adjusted to reproduce all the details of the resonances and to span the whole energy range needed to calculate the rate coefficients with high confidence up to 100 K. Details of calculations are given in Table 1. At collisional energies $E_{\rm coll}$ where resonances become negligible, the CS approximation was employed to save computing time. The CS approximation is expected to become reliable at collision energies above ~100 cm^{-1} (e.g. Phillips et al. 1996). The accuracy of CS calculations was actually checked against CC calculations and it was found necessary in practice to scale the CS cross sections, as done previously by Dubernet & Grosjean (2002). We note, however, that the contribution of the CS cross sections is only a small fraction of the thermal averages reported here. Finally, it should be noted that transitions between $J_2 = 0$ and $J_2 = 2$ (at collision energies above the J_2 channel, i.e. $E_{\rm coll} > 365$ cm^{-1}) were found to make a negligible contribution in the temperature range 5−100 K. In other words, at these temperatures, collisions can be considered as elastic for H_2 in a very good approximation. As a result, the J_2 quantum number is omitted when labeling the transitions, and the rate coefficients reported below do rigorously satisfy the detailed balance principle.

3. Results

3.1. Cross sections and rate coefficients

Figure 4 shows examples of cross sections for the rotational excitation of H_2CO by para-H_2 ($J_2 = 0$) and ortho-H_2($J_2 = 1$). These plots underline the importance of using an energy grid that is fine enough to properly describe the resonances (of both shape and Feshbach type), especially in the case of para-H_2, which generally has smaller rotational cross sections than ortho-H_2. The larger cross sections of ortho-H_2 actually reflect the importance of the interaction between the H_2CO dipole and the H_2 quadrupole, which vanishes when H_2 is in its $J_2 = 0$ level. This was previously observed for the similar H_2O−H_2 system (see Faure et al. 2007, and references therein). This effect varies greatly with transitions (e.g. the exception $1_{11} \rightarrow 4_{14}$) and is minor for molecules with small dipoles such as CO (Wernli et al. 2006).

We compare in Table 2 a sample of the present collisional rates with those of Green (1991) at two temperatures (10 and 50 K). It should be noted that in the following the He rates of Green (1991) have been scaled by the reduced mass ratio of $(\mu_{H_2CO-He}/\mu_{H_2CO-H_2})^{1/2} = 1.37$, as reported for example in the *Leiden Atomic and Molecular DataBase*[1]. We first note significant discrepancies between the present rates and those of Green (1991), either when the collider is para-H_2 or ortho-H_2. Differences are thus found to exceed a factor of 10 in some cases, e.g. for the transition $5_{14} \rightarrow 1_{11}$ at 10 K. Such discrepancies were expected since the PES employed here is very different from that employed by Green (1991) (see Sect. 2.1). However, it is striking that the differences actually do not exceed a factor of ~3 for the highest rates. We are thus compelled to conclude that the much more attractive potential well of H_2CO−H_2 compared to that of H_2CO−He does not induce dramatic effects on scattering cross sections. In this respect, the present system presents similarities with HC_3N−H_2 for which geometric aspects were found to dominate details of the PES (Wernli et al. 2007a,b). Our results also suggest that the reduced mass ratio of 1.37 is insufficient to qualitatively account for the substitution of H_2 by He. Thus, even if the differences between He and H_2 rates do

[1] http://www.strw.leidenuniv.nl/moldata/

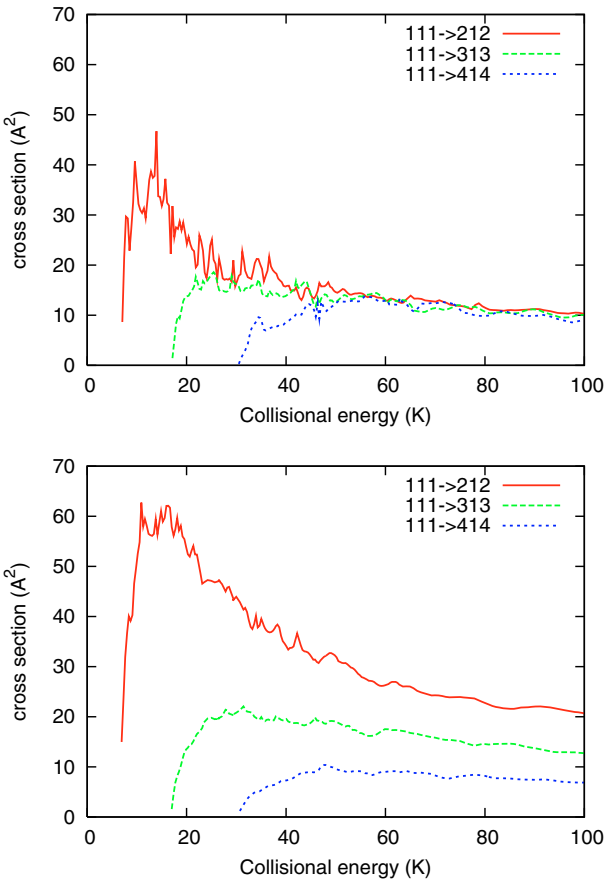

Fig. 4. Cross sections for the rotational excitation of H_2CO by para- (*upper panel*) and ortho-H_2 (*lower panel*).

Table 2. Rate coefficients for the rotational deexcitation of H_2CO by collisions with He (scaled), para-H_2 (J_2=0), and ortho-H_2 (J_2=1) at T=10 and 50 K[a].

		this work		
initial	final	He	para-H_2	ortho-H_2
		temperature = 10 K		
1_{10}	1_{11}	0.870(–10)	0.842(–10)	0.224(–09)
2_{12}	1_{11}	0.670(–10)	0.841(–10)	0.159(–09)
2_{11}	1_{11}	0.370(–10)	0.596(–10)	0.813(–10)
3_{13}	1_{11}	0.230(–10)	0.542(–10)	0.653(–10)
3_{12}	1_{11}	0.350(–11)	0.289(–10)	0.391(–10)
4_{14}	1_{11}	0.170(–10)	0.396(–10)	0.303(–10)
4_{13}	1_{11}	0.290(–11)	0.121(–10)	0.180(–10)
5_{15}	1_{11}	0.460(–11)	0.102(–10)	0.211(–10)
5_{14}	1_{11}	0.820(–12)	0.941(–11)	0.102(–10)
		temperature = 50 K		
1_{10}	1_{11}	0.550(–10)	0.522(–10)	0.177(–09)
2_{12}	1_{11}	0.510(–10)	0.639(–10)	0.134(–09)
2_{11}	1_{11}	0.340(–10)	0.577(–10)	0.670(–10)
3_{13}	1_{11}	0.220(–10)	0.459(–10)	0.584(–10)
3_{12}	1_{11}	0.530(–11)	0.198(–10)	0.291(–10)
4_{14}	1_{11}	0.150(–10)	0.343(–10)	0.267(–10)
4_{13}	1_{11}	0.510(–11)	0.892(–11)	0.139(–10)
5_{15}	1_{11}	0.440(–11)	0.958(–11)	0.180(–10)
5_{14}	1_{11}	0.150(–11)	0.571(–11)	0.675(–11)

[a] The two first columns are respectively the initial and final state of formaldehyde. Powers of ten are given in parenthesis.

not vary uniformly with transitions and temperatures, a scaling factor of ∼2−3 would be more appropriate. We emphasize in this context that Green (1991) actually recommends a scaling factor of 2.2, based on pressure-broadening measurements and theoretical calculations on NH_3. A scaling factor of ∼2.8 was reported from the low temperature measurements of Mengel & De Lucia (2000).

In Fig. 5, deexcitation rates are plotted as functions of temperature for the three colliders: He (scaled), para-H_2 (J_2=0), and ortho-H_2 (J_2 = 1). This figure clearly illustrates that a simple scaling of He rates is inappropriate for representing H_2 as the relative differences between He, para-H_2, or ortho-H_2 is significantly different from one transition to another. As a result, it appears that the substitution of H_2 by He is generally not adequate if an accuracy better than a factor of 2 is desired. On the other hand, the situtation is expected to improve at high temperatures where kinematic effects become dominant (Faure et al. 2007).

Finally, it is interesting to briefly discuss the collisional propensity rules. Despite no rigorous selection rules hold for inelastic collisions, we observed that the most probable transitions are in most cases those for which the change in angular momentum is preferentially oriented along the direction of greatest moment of inertia (the c axis). For example, the transition $1_{11} \rightarrow 2_{12}$ is preferred to $1_{11} \rightarrow 2_{11}$ (see Table 2). Similarly, we have found that the transition $1_{10} \rightarrow 2_{12}$ is preferred to $1_{11} \rightarrow 2_{11}$ (both are dipole-forbidden). This result was actually predicted by Townes & Cheung (1969) at the classical level of theory and shown to explain the cooling of the excitation temperatures of both the 6-cm and 2-cm doublets (transitions $1_{10} \rightarrow 1_{11}$ and $2_{11} \rightarrow 2_{12}$, respectively). It should be noted, however, that this propensity fails for some transitions and that its strength depends on the collider and, to a lesser extent, on the temperature (see Table 2 and also Sect. 4). Moreover, the propensity is generally stronger for He than for H_2, reflecting significant differences in the corresponding interactions. We thus conclude that the ratios of rates for dipole-forbidden transitions, which are essential for the cooling of the doublets, do vary significantly from one collider to another. This important issue will be discussed in details, through radiative transfer modeling, in a forthcoming paper.

3.2. Fitting procedure and critical density

For use in astrophysical modeling, the rotational transition rates $R(J_{K_aK_c} \rightarrow J'_{K'_aK'_c}, T)$ must be evaluated on a sufficiently fine temperature grid. The rates were therefore least-square fitted over the temperature range 5−100 K by the analytic form used by Faure et al. (2004):

$$\log_{10} R(J_{K_aK_c} \rightarrow J'_{K'_aK'_c}, T) = \sum_{n=0}^{4} a_n T^{-n/6}. \quad (1)$$

The results of the fits are summarized in Tables 5 and 6. The fitting accuracy was found to be better than 0.1%.

To quantitatively assess the impact of the new H_2CO-H_2 collisional rates on formaldehyde emission, detailed radiative transfer studies adapted to various astronomical environments are required. In Sect. 4 below, this impact is investigated for a range of density and temperature conditions by neglecting all excitation mechanisms other than the 2.7 K Cosmic Microwave Background (CMB) radiation and H_2 collisions. A first-order indicator is also provided by the impact of rates on critical

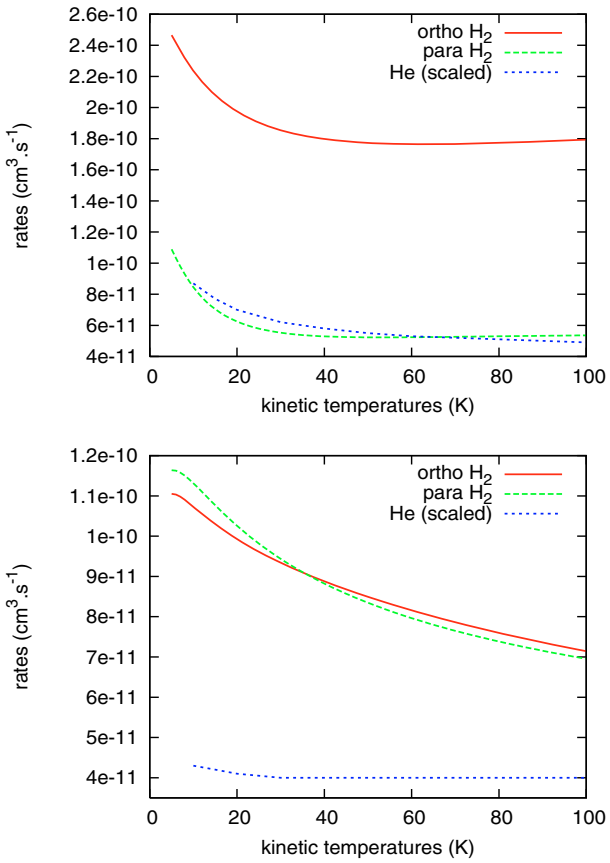

Fig. 5. Rate coefficients for the rotational transitions $1_{10} \rightarrow 1_{11}$ (*upper panel*) and $2_{12} \rightarrow 1_{10}$ (*lower panel*) as functions of temperature for (scaled) He (Green 1991), para-H_2 ($J_2 = 0$) and ortho-H_2 ($J_2 = 1$).

densities. For a multi-level system, the critical density of a given partner (here He, para- or ortho-H_2) is usually defined (neglecting absorption and induced emission) as the density at which the sum of the collisional de-excitation rates of a given level is equal to the sum of the spontaneous radiative de-excitation rates:

$$n_{\rm cr}(J_{K_aK_c}, T) = \frac{\Sigma_{J'_{K'_aK'_c}} A(J_{K_aK_c} \rightarrow J'_{K'_aK'_c})}{\Sigma_{J'_{K'_aK'_c}} R(J_{K_aK_c} \rightarrow J'_{K'_aK'_c}, T)} \,. \quad (2)$$

When the colliding partner has a density $n \gg n_{\rm cr}$, collisions maintain rotational levels in local thermodynamic equilibrium (LTE) at the kinetic temperature. When $n \ll n_{\rm cr}$, the rotational levels are in LTE at the temperature of the background radiation (here the 2.7 K CMB). The effect of collisions is important for densities $n \sim n_{\rm cr}$, where deviations from LTE occurred, including population inversions. Equation (2) was computed using Einstein coefficients from the *Cologne Database for Molecular Spectroscopy*[2]. Results are presented in Table 3 for the 5 lowest upper doublet levels of ortho-formaldehyde. Is is observed that critical densities for H_2 are decreased with respect to the scaled He values by a typical factor of 2−3. These differences obviously reflect the impact of the new rates, although rotational rates are summed here over all possible downward transitions, thus averaging their effect. Greater differences in emission line fluxes are thus expected as individual state-to-state rates can exceed the scaled He values by more than an order of magnitude. This is demonstrated in Sect. 4 below. Level 1_{10} has a much lower critical density than the other levels owing to the single allowed radiative transition $1_{10} - 1_{11}$.

[2] http://www.ph1.uni-koeln.de/vorhersagen/

Table 3. Critical densities, in cm^{-3}, for (scaled) He, para-H_2 ($J_2 = 0$), and ortho-H_2 ($J_2 = 1$), as functions of temperature for the 5 lowest upper doublet levels of ortho-formaldehyde[a].

$J_{K_aK_c}$	T(K)	He	p-H_2	o-H_2	He/p-H_2	He/o-H_2
1_{10}	10	4.1(01)	4.2(01)	1.6(01)	0.97	2.6
	50	6.5(01)	6.9(01)	2.0(01)	0.94	3.3
	100	7.3(01)	6.7(01)	2.0(01)	1.09	3.7
2_{11}	10	4.3(05)	3.3(05)	1.8(05)	1.3	2.4
	50	6.3(05)	2.2(05)	4.2(05)	2.9	1.5
	100	6.3(05)	2.3(05)	4.4(05)	2.7	1.4
3_{12}	10	2.1(06)	1.0(06)	6.8(05)	2.1	3.1
	50	2.3(06)	1.3(06)	7.8(05)	1.8	2.9
	100	2.2(06)	1.4(06)	8.1(05)	1.6	2.7
4_{13}	10	6.8(06)	2.2(06)	1.7(06)	3.1	4.0
	50	6.0(06)	2.7(06)	1.8(06)	2.2	3.3
	100	5.2(06)	3.0(06)	1.9(06)	1.7	2.7
5_{14}	10	9.5(06)	4.1(06)	3.4(06)	2.3	2.8
	50	1.0(07)	4.8(06)	3.4(06)	2.1	2.9
	100	9.5(06)	5.3(06)	3.4(06)	1.8	2.8

[a] Powers of 10 are given in parentheses. See text for details.

Table 4. Formaldehyde lines selected in Fig. 6. See text for details.

transition	ν(GHz)	$E_{\rm up}$ (K)
$2_{12} \rightarrow 1_{11}$	140.8	22.64
$2_{11} \rightarrow 1_{10}$	150.4	21.95
$3_{13} \rightarrow 2_{12}$	211.2	32.09
$3_{12} \rightarrow 2_{11}$	225.6	33.48
$4_{14} \rightarrow 3_{13}$	281.5	45.62
$4_{13} \rightarrow 3_{12}$	300.8	47.94
$5_{15} \rightarrow 4_{14}$	351.7	62.52
$5_{14} \rightarrow 4_{13}$	375.8	65.99

4. Modeling formaldehyde emission

In this section we investigate the impact of the new computed collisional coefficients on the theoretical predictions of formaldehyde line emission. We employed the MOLPOP program, written by Moshe Elitzur & Philip Lockett, to solve the radiative transfer equations using the escape probability method for a homogeneous slab (e.g. Krolik & McKee 1978). We consider the 10 first levels of ortho-H_2CO ($E_{\rm up} \leq 46$ cm^{-1}, see Fig. 3) and the 8 most intense millimeter transitions, as reported in Table 4. The computed line spectrum depends on the following basic parameters: the density of the colliders (here para and/or ortho-H_2), the kinetic temperature, the formaldehyde column density, and the linewidth. To have a relatively exhaustive study, we explored a large parameter space by varying the H_2 density between 10 and 10^8 cm^{-3}, the kinetic temperature between 10 and 30 K, the formaldehyde column density between 10^{13} and 10^{15} cm^{-2}, keeping the Doppler linewidth equal to 1 km s^{-1}. We thus considered both optically thin and optically thick lines. Finally, we included the 2.7 K CMB radiation field,

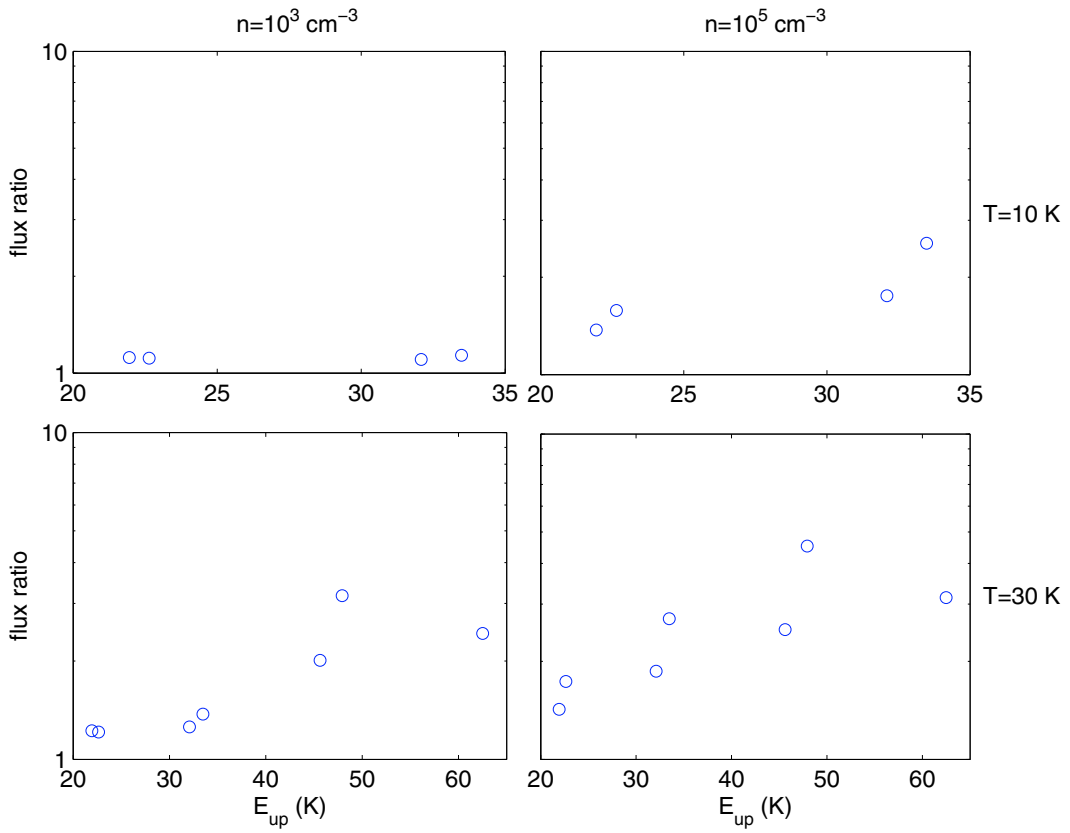

Fig. 6. Emission-line flux ratios from escape-probability modeling as functions of the upper energy levels of ortho-H_2CO for representative densities and temperatures. Two differents sets of collision rates were employed (see text for details). The H_2CO column density is fixed at 5×10^{13} cm^{-2}, corresponding to an optical depth of 1 for the $2_{12} \rightarrow 1_{11}$ transition. Open circles denote the ratios between line fluxes based on the present ortho-H_2 rates and fluxes based on the (scaled) He rates of Green (1991). The plotted ratios correspond to transitions whose fluxes are more than 1% of the total flux (summed over all millimeter transitions). Transitions can be identified from the upper energies given in Table 4. The weakest plotted line (T = 10 K, $n = 10^3$ cm^{-3}, E_{up} = 33.48 K) has an antenna temperature of 10 mK.

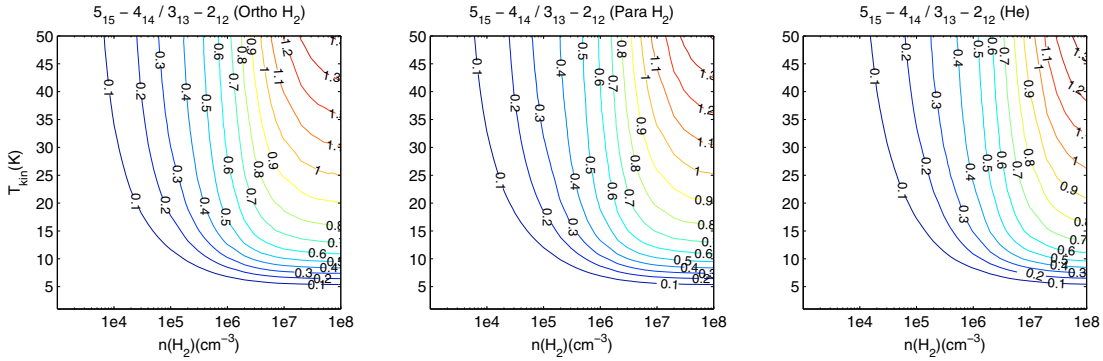

Fig. 7. Variation of the line antenna temperature ratio $(5_{15} \rightarrow 4_{14})/(3_{13} \rightarrow 2_{12})$ with kinetic temperature and H_2 density. The column density is fixed at 1.5×10^{14}, as in van Dishoeck et al. (1995). The colliders are ortho-H_2 (*left panel*); para-H_2 (*middle panel*); scaled He (*right panel*).

but all other possible sources of radiation were neglected to focus on the effect of collisions.

Escape probability computations were performed using two sets of collisional data: the scaled H_2CO-He rates of Green (1991) and the present H_2CO–H_2 rates. The results of this comparison are reported in Fig. 6, where we show the relevant line flux ratios for ortho-H_2CO at representative densities and temperatures. Only collision rates with ortho-H_2 are considered to simplify the interpretation. The H_2CO column density is fixed at 5×10^{13} cm^{-2}. It can be observed that line fluxes based on the present rates are increased up to a factor of 5 with respect to fluxes based on the scaled He rates of Green (1991). These results clearly reflect the differences in collisional rates (see Table 2). They also show that inaccuracies in rates are not amplified but are quasi-linearly propagated within the radiative transfer equations. In particular, it is worth noting that the typical increase in fluxes at 30 K is less than a factor of 2–3 at the investigated densities. Similar results were obtained with para-H_2. We also observe that the flux ratios rise with increasing upper energies. This was expected since the critical densities are higher for

Table 5. Coefficients a_i of the polynomial fit, Eq. (1), to the rotational de-excitation rate coefficients of ortho-H_2CO by para-H_2 ($J_2 = 0$). These coefficients are only valid in the temperature range 5−100 K. $E_{up}(K)$ are the upper level energies.

i	f	$E_{up}(K)$	$a0$	$a1$	$a2$	$a3$	$a4$
1_{10}	1_{11}	15.4	–15.992	49.730	–153.065	198.787	–91.799
2_{12}	1_{11}	21.9	–14.123	24.535	–59.587	65.932	–27.196
2_{12}	1_{10}	21.9	–10.062	–5.315	20.538	–25.241	10.146
2_{11}	1_{11}	22.6	–12.447	18.170	–51.831	61.863	–26.279
2_{11}	1_{10}	22.6	–13.020	22.100	–66.801	87.006	–40.604
2_{11}	2_{12}	22.6	–8.383	–14.613	34.590	–30.732	8.751
3_{13}	1_{11}	32.1	–10.998	2.989	–6.021	6.833	–3.110
3_{13}	1_{10}	32.1	–11.265	–3.697	24.981	–36.985	16.872
3_{13}	2_{12}	32.1	–11.560	8.307	–18.749	20.791	–9.220
3_{13}	2_{11}	32.1	–8.857	–14.745	45.725	–54.400	22.643
3_{12}	1_{11}	33.4	–7.959	–18.565	41.867	–37.082	10.967
3_{12}	1_{10}	33.4	–7.167	–21.051	50.053	–52.574	20.559
3_{12}	2_{12}	33.4	–7.585	–15.765	31.555	–25.252	6.789
3_{12}	2_{11}	33.4	–9.219	–7.709	19.526	–19.440	6.651
3_{12}	3_{13}	33.4	–6.861	–28.383	76.268	–82.840	31.812
4_{14}	1_{11}	45.6	–8.420	–22.040	70.489	–89.088	39.395
4_{14}	1_{10}	45.6	–8.879	–11.776	25.407	–21.517	5.965
4_{14}	2_{12}	45.6	–8.358	–14.534	37.209	–39.039	14.521
4_{14}	2_{11}	45.6	–9.156	–16.688	57.442	–74.097	32.875
4_{14}	3_{13}	45.6	–6.813	–25.619	71.485	–84.483	35.717
4_{14}	3_{12}	45.6	–7.516	–24.778	71.169	–81.492	32.987
4_{13}	1_{11}	47.9	0.146	–75.208	182.668	–190.508	72.556
4_{13}	1_{10}	47.9	–0.562	–71.751	179.682	–192.438	75.030
4_{13}	2_{12}	47.9	–4.468	–44.470	112.705	–120.438	46.436
4_{13}	2_{11}	47.9	–6.130	–27.069	64.616	–67.231	25.710
4_{13}	3_{13}	47.9	–3.286	–47.389	113.572	–115.674	42.566
4_{13}	3_{12}	47.9	–7.831	–19.582	56.982	–68.227	29.130
4_{13}	4_{14}	47.9	–6.043	–37.551	106.355	–122.270	49.757
5_{15}	1_{11}	62.5	–2.885	–56.794	144.040	–157.327	62.568
5_{15}	1_{10}	62.5	–8.540	–20.660	65.931	–83.981	37.484
5_{15}	2_{12}	62.5	–5.528	–40.839	116.705	–139.479	59.605
5_{15}	2_{11}	62.5	–5.043	–40.949	105.056	–114.675	45.381
5_{15}	3_{13}	62.5	–9.080	–8.966	23.299	–24.102	8.563
5_{15}	3_{12}	62.5	–7.782	–25.906	80.727	–100.299	43.864
5_{15}	4_{14}	62.5	–8.105	–17.309	53.010	–67.438	30.101
5_{15}	4_{13}	62.5	–7.878	–23.580	69.113	–79.281	31.954
5_{14}	1_{11}	65.9	23.067	–227.845	554.740	–587.588	229.569
5_{14}	1_{10}	65.9	5.613	–114.856	283.950	–302.641	118.131
5_{14}	2_{12}	65.9	2.003	–92.221	234.680	–255.324	101.243
5_{14}	2_{11}	65.9	–2.865	–56.224	145.705	–160.954	64.718
5_{14}	3_{13}	65.9	–0.118	–75.765	195.552	–215.974	86.951
5_{14}	3_{12}	65.9	–4.075	–39.992	96.701	–102.708	40.144
5_{14}	4_{14}	65.9	–2.837	–52.566	130.263	–136.923	52.129
5_{14}	4_{13}	65.9	–8.376	–14.931	44.661	–54.560	23.598
5_{14}	5_{15}	65.9	–4.370	–49.693	138.072	–159.025	65.670

higher levels (see Table 3). Furthermore, it can be noticed that the flux ratios are higher for the upper level than for the lower level of a doublet. This again shows that the propensity rule discussed in Sect. 3.1 (at the origin of the cooling of the 6-cm and 2-cm transitions) is stronger for He than for ortho-H_2.

Finally, Fig. 7 shows the variation of the line ratio ($5_{15} \rightarrow 4_{14}$)/($3_{13} \rightarrow 2_{12}$) with kinetic temperature and H_2 density for the three colliding partners He, para-H_2, and ortho-H_2. Such plots have been previously employed to use H_2CO as a "densitometer" (e.g. van Dishoeck et al. 1995). As we can see, for a given line ratio, the present H_2 rates lead to kinetic temperatures and H_2 densities lower than those obtained with (scaled) He rates. For instance, for a kinetic temperature of 15 K and an H_2 density of 10^6 cm^{-3}, the line ratio increases from 0.3 for He to 0.45 for para-H_2 and 0.48 for ortho-H_2. These effects are explained well by the differences between the corresponding rates, H_2 rates being generally higher than those for He (see Sect. 3). We conclude that the present rates will significantly improve the accuracy of H_2 densities derived from H_2CO millimeter observations. For temperatures above 30 K, levels above the lowest 10 can be required to converge the radiative transfer equations. Results in Fig. 7 are therefore only indicative for $T > 30$ K.

5. Conclusions

We have computed rate coefficients for the rotational (de)excitation of ortho-H_2CO colliding with both para-H_2 ($J = 0$) and ortho-H_2 ($J = 1$) for kinetic temperatures in the range 5−100 K. All transitions among the 10 lowest levels of ortho-H_2CO ($E_{up} \leq 46$ cm^{-1}) were considered. Fully converged quantum scattering calculations were run on a high-accuracy H_2CO−H_2 PES determined at the CCSD(T) level with a basis

Table 6. Coefficients a_i of the polynomial fit, Eq. (1), to the rotational de-excitation rate coefficients of ortho-H_2CO by ortho-H_2 ($J_2 = 1$). These coefficients are only valid in the temperature range 5−100 K. $E_{up}(K)$ are the upper level energies.

i	f	$E_{up}(K)$	$a0$	$a1$	$a2$	$a3$	$a4$
1_{10}	1_{11}	15.4	–5.246	–25.463	50.646	–41.276	11.552
2_{12}	1_{11}	21.9	–4.448	–34.039	77.211	–74.951	26.474
2_{12}	1_{10}	21.9	–15.045	27.704	–59.603	59.399	–22.826
2_{11}	1_{11}	22.6	–13.581	26.572	–76.172	94.542	–42.485
2_{11}	1_{10}	22.6	–3.911	–37.123	83.373	–80.136	27.979
2_{11}	2_{12}	22.6	–4.098	–38.832	91.173	–90.833	32.780
3_{13}	1_{11}	32.1	–12.249	9.069	–14.678	10.580	–3.009
3_{13}	1_{10}	32.1	–12.048	4.950	–3.851	0.604	–0.052
3_{13}	2_{12}	32.1	–3.167	–42.183	99.491	–102.666	39.005
3_{13}	2_{11}	32.1	–11.687	2.740	6.478	–16.171	8.844
3_{12}	1_{11}	33.4	–8.713	–17.582	51.180	–58.548	23.406
3_{12}	1_{10}	33.4	–10.444	2.041	–9.473	15.830	–8.742
3_{12}	2_{12}	33.4	–7.197	–19.667	43.764	–39.570	12.288
3_{12}	2_{11}	33.4	–2.386	–47.324	111.029	–113.372	42.396
3_{12}	3_{13}	33.4	–2.975	–50.456	126.727	–135.282	52.361
4_{14}	1_{11}	45.6	–9.339	–13.114	40.769	–49.568	20.912
4_{14}	1_{10}	45.6	–5.796	–38.988	109.015	–126.546	52.590
4_{14}	2_{12}	45.6	–11.270	3.006	1.814	–10.423	6.826
4_{14}	2_{11}	45.6	–8.709	–17.808	55.011	–66.190	27.762
4_{14}	3_{13}	45.6	–1.835	–51.135	123.109	–130.486	50.953
4_{14}	3_{12}	45.6	–9.636	–13.173	49.472	–66.031	29.871
4_{13}	1_{11}	47.9	1.815	–84.457	204.979	–214.958	82.678
4_{13}	1_{10}	47.9	–6.494	–35.500	99.787	–116.056	48.209
4_{13}	2_{12}	47.9	–5.956	–37.630	104.313	–119.372	48.835
4_{13}	2_{11}	47.9	–9.326	–7.028	19.235	–21.708	8.395
4_{13}	3_{13}	47.9	–4.439	–42.170	107.517	–116.637	45.968
4_{13}	3_{12}	47.9	–1.072	–55.924	134.023	–141.311	54.892
4_{13}	4_{14}	47.9	–2.571	–56.264	146.562	–161.996	64.975
5_{15}	1_{11}	62.5	–2.435	–61.106	160.877	–180.996	74.047
5_{15}	1_{10}	62.5	–7.115	–27.779	74.426	–83.817	33.844
5_{15}	2_{12}	62.5	–6.977	–31.392	92.626	–112.192	48.275
5_{15}	2_{11}	62.5	–5.037	–43.501	119.662	–137.899	57.159
5_{15}	3_{13}	62.5	–9.789	–6.265	24.609	–35.514	17.167
5_{15}	3_{12}	62.5	–7.974	–23.986	72.798	–87.731	37.206
5_{15}	4_{14}	62.5	–0.836	–56.961	137.327	–147.020	58.139
5_{15}	4_{13}	62.5	–9.190	–16.967	59.313	–76.718	34.145
5_{14}	1_{11}	65.9	–5.756	–47.108	134.586	–156.999	65.159
5_{14}	1_{10}	65.9	8.987	–134.997	333.074	–356.819	140.618
5_{14}	2_{12}	65.9	4.663	–105.646	262.859	–283.286	112.095
5_{14}	2_{11}	65.9	–4.445	–46.939	126.569	–144.623	59.698
5_{14}	3_{13}	65.9	–4.927	–45.527	125.394	–143.484	58.809
5_{14}	3_{12}	65.9	–7.968	–16.284	44.436	–51.820	21.664
5_{14}	4_{14}	65.9	–3.761	–49.146	129.223	–144.139	58.274
5_{14}	4_{13}	65.9	–0.025	–61.370	145.659	–153.236	59.579
5_{14}	5_{15}	65.9	–3.379	–51.906	137.072	–153.041	61.860

set extrapolation procedure. The present rates are thus expected to be accurate to ∼10%. Large differences with the (scaled) H_2CO–He rates of Green (1991) were observed and emission line fluxes, computed *via* the escape probability method, were shown to be increased by up to a factor of 5. Moreover, the strength of propensity rules was found to depend on the collider. The present rates should therefore be adopted in any detailed radiative transfer model of ortho-H_2CO in cold environments, typically $T \lesssim 30$ K. Previously published H_2CO abundance and H_2 density estimates should be revised accordingly.

In a forthcoming publication (Troscompt et al., in preparation), we will investigate the impact of these new rates on the cooling of the 6-cm doublet excitation temperature (transition $1_{10} \rightarrow 1_{11}$), which has been used so far as a sensitive probe of the coldest and darkest interstellar sources. For warmer environments ($T \gtrsim 30$ K), rates for higher-lying levels are required and further scattering calculations are planned at lower accuracy as close-coupling calculations become prohibitive. Calculations on para-H_2CO are also currently under progress. All rate data will be made available in the BASECOL database (http://www.obspm.fr/basecol/) and at the CDS (http://cdsweb.u-strasbg.fr/).

Acknowledgements. All scattering calculations were performed on the *Service Commun de Calcul Intensif de l'Observatoire de Grenoble* with the valuable help of F. Roch. Ab initio CCSD(T)/aug-cc-pVTZ and R12 calculations were performed on the IDRIS and CINES French national computing centers. This research was supported by the CNRS national program "Physique et Chimie du Milieu Interstellaire" and by the FP6 Research Training Network "Molecular Universe" (contract number MRTN-CT-2004-512302).

References

Alexander, M., & Manolopoulos, D. 1987, J. Chem. Phys., 86
Augustin, S. D., & Miller, W. H. 1974, J. Chem. Phys., 61
Bacmann, A., Lefloch, B., Ceccarelli, C., et al. 2003, ApJ, 585, L55
Bocquet, R. E. A. 1996, J. Mol. Spec., 177, 154
Cazaux, S., Tielens, A. G. G. M., Ceccarelli, C., et al. 2003, ApJ, 593, L51
Ceccarelli, C., Loinard, L., Castets, A., Tielens, A. G. G. M., & Caux, E. 2000, A&A, 357, L9
Ceccarelli, C., Loinard, L., Castets, A., et al. 2001, A&A, 372, 998
Ceccarelli, C., Maret, S., Tielens, A. G. G. M., Castets, A., & Caux, E. 2003, A&A, 410, 587
Clouthier, D. J., & Ramsey, D. A. 1983, Ann. Rev. Phys. Chem., 34, 31
Dubernet, M.-L., & Grosjean, A. 2002, A&A, 390, 793
Dubernet, M. L., Daniel, F., Grosjean, A., et al. 2006, A&A, 460, 323
Duncan, J. L. 1974, Mol. Phys., 28, 1177
Faure, A., & Wiesenfeld, L. 2004, J. Chem. Phys., 121, 6771
Faure, A., Gorfinkiel, J. D., & Tennyson, J. 2004, MNRAS, 347, 323
Faure, A., Valiron, P., Wernli, M., et al. 2005, J. Chem. Phys., 122, 1102
Faure, A., Crimier, N., Ceccarelli, C., et al. 2007, A&A, 472, 1029
Fray, N., Bénilan, Y., Biver, N., et al. 2006, Icarus, 184, 239
Garrison, B. J., & Lester, Jr., W. A. 1975, J. Chem. Phys., 63, 4167
Garrison, B. J., Lester, Jr., W. A., & Miller, W. H. 1976, J. Chem. Phys., 65, 2193
Garrison, B. J., Lester, Jr., W. A., Miller, W. H., & Green, S. 1975, ApJ, 200, L175
Green, S. 1991, ApJS, 76, 979
Green, S., Garrison, B. J., Lester, Jr., W. A., & Miller, W. H. 1978, ApJS, 37, 321
Hutson, J. M., & Green, S. 1994, MOLSCAT computer code, version 14, distributed by Collaborative Computational Project No. 6 of the Engineering and Physical Sciences Re search Council UK
Jankowski, P., & Szalewicz, K. 2005, J. Chem. Phys., 123, 4301
Kaur, S., & Baluja, K. L. 2005, J. Phys. B Atom. Mol. Phys., 38, 3917
Krolik, J. H., & McKee, C. F. 1978, ApJS, 37, 459
Lique, F., Senent, M.-L., Spielfiedel, A., & Feautrier, N. 2007, J. Chem. Phys., 126, 4312
Liszt, H. S., Lucas, R., & Pety, J. 2006, A&A, 448, 253
Mangum, J. G., Darling, J., Menten, K. M., & Henkel, C. 2008, ApJ, 673, 832
Mangum, J. G., & Wootten, A. 1993, ApJS, 89, 123
Maret, S., Ceccarelli, C., Caux, E., et al. 2004, A&A, 416, 577
Mengel, M., & De Lucia, F. C. 2000, ApJ, 543, 271
Minh, Y. C., Irvine, W. M., & McGonagle, D. 1993, J. Kor. Astro. Soc., 26, 99
Noga, J., & Kutzelnigg, W. 1994, J. Chem. Phys., 101, 7738
Noga, J., Kallay, M., & Valiron, P. 2006, Mol. Phys., 104, 2337
Phillips, T. R., Maluendes, S., & Green, S. 1996, ApJS, 107, 467
Phillips, T. R., Maluendes, S., McLean, A. D., & Green, S. 1994, J. Chem. Phys., 101, 5824
Snyder, L. E., Buhl, D., Zuckerman, B., & Palmer, P. 1969, Phys. Rev. Lett., 22, 679
Townes, C. H., & Cheung, A. C. 1969, ApJ, 157, L103
Valiron, P., Wernli, M., Faure, A., et al. 2008, J. Chem. Phys., 129, 134306
van der Tak, F. F. S., van Dishoeck, E. F., & Caselli, P. 2000, A&A, 361, 327
van Dishoeck, E. F., Blake, G. A., Jansen, D. J., & Groesbeck, T. D. 1995, ApJ, 447, 760
Wernli, M., Valiron, P., Faure, A., et al. 2006, A&A, 446, 367
Wernli, M., Wiesenfeld, L., Faure, A., & Valiron, P. 2007a, A&A, 475, 391
Wernli, M., Wiesenfeld, L., Faure, A., & Valiron, P. 2007b, A&A, 464, 1147
Wheeler, M. D., & Ellis, A. M. 2003, Chem. Phys. Lett., 374, 392
Williams, H. L., Mas, E. M., Szalewicz, K., & Jeziorski, B. 1995, J. Chem. Phys., 103, 7374